

# $^{252}\text{Cf}$ Fission Fragment Ionization Mass Spectrometry of Chlorophyll *a*

B. T. Chait\* and F. H. Field

Contribution from the Rockefeller University, New York, New York 10021.  
Received May 9, 1983

**Abstract:** The title study has been made by using a time-of-flight mass spectrometer, placing primary emphasis on fragmentation reactions and rates. The mass spectrometer was modified so that segmented fields with segments of different magnitudes could be applied in the ion acceleration region and retarding potentials in the region between the flight tube and the ion detector. Methods using these retarding potentials were developed for determining the identities of fragmentations in the flight tube and for measuring the rate constants of fragmentations occurring in the ion acceleration region. Positive and negative spectra were determined with and without retarding potentials at the end of the flight tube. Extensive amounts of fragmentation occur both close to the sample foil (prompt fragmentation) and in the flight tube. For example, 98.9% of the positive molecular ions from chlorophyll *a* entering the flight tube fragment before reaching the detector. In the spectra with retarding potential applied,  $M^+$  and  $(M + H)^+$  ions are the ions in the positive molecule-ion region, and  $(M - H)^-$ ,  $M^-$ , and  $(M + H)^-$  are the ions in the negative molecule-ion region. Networks of fragmentation paths were deduced from retarding potential measurements. Rate constants for certain fragmentations are deduced from tails on peaks and from measurements utilizing segmented fields in the ion acceleration region. It is deduced that fragmentations occur with rate constants ranging from  $>10^9 \text{ s}^{-1}$  to  $10^4 \text{ s}^{-1}$ . It is suggested that the fission fragment induced fragmentation processes observed in Chl *a* involve many of the concepts embodied in the quasi-equilibrium theory of mass spectra, e.g., formation of reactant ions with a wide range of energies, which results in a network of sequential and competing unimolecular reactions with variable and wide-ranging rate constants.

This paper is a report of our study of the mass spectra of chlorophyll *a* (Chl *a*) obtained with our fission fragment ionization mass spectrometer. Chl *a* has been resistant to treatment by conventional mass spectrometry (EI and CI) because of its low volatility and relative chemical fragility, and consequently little is known about the detailed mass spectrometry of this important compound. Recently spectra have been obtained by Hunt, Macfarlane, Katz, and Dougherty<sup>1,2</sup> using fission fragment ionization mass spectrometry (referred to by these workers as plasma desorption mass spectrometry) and by Dougherty, Dreifuss, Sphon, and Katz<sup>3</sup> using field desorption mass spectrometry. Dougherty has written two pertinent reviews of the mass spectrometry of tetrapyrroles.<sup>4,5</sup> One of the fission fragment mass spectrometry papers<sup>1</sup> is concerned mainly with chlorophyll aggregates; the field desorption paper is concerned mainly with chlorophyll hydration. The second fission fragment ionization paper treats some aspects of the ionization and fragmentation of the compound, but it is of limited extent. We had been using fission fragment mass spectrometry for the analysis of Chl *a*, and some of the hypotheses advanced in the paper were contrary to our observations. Consequently, we made an extensive study of the fission fragment ionization mass spectrometry of the compound, placing primary emphasis on fragmentation reactions and rates. It is our observation that similarities exist between the spectra produced and the processes involved in the various kinds of impact desorption mass spectrometry (fission fragment ionization, fast-atom bombardment, slow-ion bombardment, and laser desorption) and even conventional mass spectrometry (electron ionization and chemical ionization). Therefore we think that our results will be of interest in types of mass spectrometry other than fission fragment ionization. A preliminary report of our work has been published.<sup>6</sup>

## Experimental Section

The mass spectra were obtained with the time-of-flight fission fragment ionization mass spectrometer built in this laboratory and described previously.<sup>7</sup> It contains three grids in front of the ion detector, and the purpose of these is to provide a retarding potential for the study of ions produced by fragmentations occurring in the 3-m flight tube of the mass spectrometer.<sup>8</sup> It also contains three grids in the ion acceleration region. These were used to provide electric fields in the ion accelerating region which were of discontinuously different magnitudes. This in turn enabled us to make measurements of rates of ion fragmentations in the acceleration region. A schematic drawing of the apparatus is given in Figure 1. The ion acceleration voltage,  $V_s$ , applied to the sample foil was usually 10 kV.

The nominal strength of the  $^{252}\text{Cf}$  source was 45  $\mu\text{Ci}$ , and this produced a bombarding flux of 3000 fission fragments  $\text{s}^{-1}$  thru the sample foil. Samples with a surface density of approximately 15  $\mu\text{g}/\text{cm}^2$  were prepared by evaporation of Chl *a* from benzene and  $\text{CCl}_4$  solutions on 1- $\mu\text{m}$ -thick Ni and 2- $\mu\text{m}$ -thick aluminized polyester. Samples of Chl *a* were obtained from Professor D. C. Mauzerall of The Rockefeller University, the Sigma Chemical Co., St. Louis, MO, and US Biochemical Corp., Cleveland, OH. The spectra from all samples were essentially identical, except for some variation in the pheophytin *a* (Chl *a* - Mg + 2H) content. The presence of pheophytin *a* was easily detected from the mass spectra. Solutions were made up in the laboratory atmosphere working as rapidly as possible, and these solution were dropped on the sample foils as rapidly as possible. The solvent was evaporated from the foils by evacuation, and the sample foils thus prepared were rapidly transferred to the mass spectrometer.

The fission fragment ionization mass spectra obtained in a time-of-flight mass spectrometer exhibit many peaks that are quite broad by conventional mass spectrometric standards, and these peaks often exhibit wings and tails. We pointed out in an earlier work<sup>8</sup> that the broadening of peaks may be ascribed to the occurrence of fragmentations in the flight tube, and the tails may be ascribed to fragmentations in the ion acceleration region. Fragmentations often entail the conversion of internal energy to kinetic energy of the fragments, and when the fragmentations occur in the flight tube this kinetic energy produces fragment ions with a distribution of velocities and, consequently, of flight times. When the fragmentations occur in the ion acceleration region the conversion of internal energy to kinetic energy is of much less importance than the fact that fragmentations occurring at different places in the strong electric field in the acceleration region will produce ions with differing flight

(1) Hunt, J. E.; Macfarlane, R. D.; Katz, J. J.; Dougherty, R. C. *Proc. Natl. Acad. Sci. U.S.A.* **1980**, *77*, 1745.

(2) Hunt, J. E.; Macfarlane, R. D.; Katz, J. J.; Dougherty, R. C. *J. Am. Chem. Soc.* **1981**, *103*, 6775.

(3) Dougherty, R. C.; Dreifuss, P. A.; Sphon, J.; Katz, J. J. *J. Am. Chem. Soc.* **1980**, *102*, 416.

(4) Dougherty, R. C. In "Biochemical Applications of Mass Spectrometry"; Waller, G. R., Ed.; Wiley-Interscience: New York, 1972; pp 591-600.

(5) Dougherty, R. C. In "Biochemical Applications of Mass Spectrometry"; Waller, G. R., Dermer, O. C., Eds.; Wiley: New York, 1980; 1st Suppl. Vol., pp 693-701.

(6) Chait, B. T.; Field, F. H. *J. Am. Chem. Soc.* **1982**, *104*, 5519.

(7) Chait, B. T.; Agosta, W. C.; Field, F. H. *Int. J. Mass Spectrom. Ion Phys.* **1981**, *39*, 339.

(8) Chait, B. T.; Field, F. H. *Int. J. Mass Spectrom. Ion Phys.* **1981**, *41*, 17.

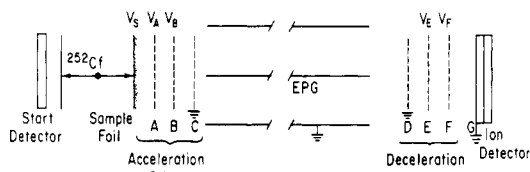


**Figure 1.** Fission fragment ionization MS. EPG is the electrostatic particle guide, which enhances transport of ions down the flight tube. Intergrid distances (in mm):  $d_{\text{foil-A}} = 3.5$ ,  $d_{\text{A-B}} = 6.4$ ,  $d_{\text{B-C}} = 6.4$ ,  $d_{\text{D-E}} = 8.7$ ,  $d_{\text{E-F}} = 11.9$ , and  $d_{\text{F-G}} = 6.3$ .

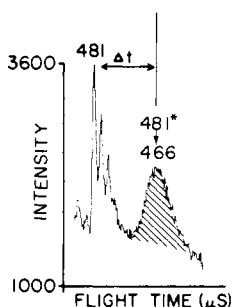


**Figure 2.** Separation of peak from flight-tube fragmentation ions (crosshatched) from sharp peaks from ions not fragmenting in the flight tube. The decomposition involved in the crosshatched peak is  $m/z$  481  $\rightarrow$   $m/z$  466.

times. An immediate result of these fragmentations is a serious degradation of the resolution of the time-of-flight mass spectrometer.

A fragment ion produced by the decomposition of a precursor ion in the flight tube of the mass spectrometer will have only a fraction of the kinetic energy of the precursor ion, and a retarding potential will exist that will allow the precursor ion to reach the detector but will stop the fragment ion. Thus the application of suitable retarding potentials can significantly sharpen spectra and increase the resolution of the spectrometer. Furthermore, if one can determine the minimum retarding potential needed to repel the fragment ion, simple kinetic energy considerations allow one to deduce the mass of the fragment ion. Since the  $m/z$  value of the broad peak under investigation gives directly the mass of the precursor ion, the minimum retarding potential gives the identity of the flight-tube fragmentation occurring.

This minimum retardation potential method for determining flight-tube ion fragmentation reactions was used in our earlier work,<sup>8</sup> but for the present work we have utilized a method<sup>9</sup> that is more accurate and experimentally easier. The method depends upon the fact that when a retarding potential is applied to deceleration grids E and F (Figure 1), ions produced by fragmentation in the flight tube are, because of their lower kinetic energy, decelerated more by a given retarding potential than ions that have not undergone decompositions in the flight tube. Consequently the flight-tube fragmentation ions move more slowly between grid D and ion detector G (Figure 1) than do the nonfragmented ions, and this in turn results in a longer total flight time for the fragment ions. Experimentally one observes that as the retarding potential is increased the broad peak produced by the flight-tube fragment ions moves away from the sharp peak(s) produced by the nonfragmented ions. This is illustrated in Figure 2 where the Chl *a* sharp peaks corresponding to the ions with  $m/z$  481, 482, and 483 are at the left, and the crosshatched broad peak corresponding to the ions formed by the decomposition of the  $m/z$  481 ion to the  $m/z$  466 ion in the flight tube is at the right. The difference between the arrival times of the fragment ions and the precursor ions is related quantitatively to the difference in mass of the two kinds of ions, and it constitutes a means for determining the nature of the fragmentation.

In these measurements deceleration grids E and F (Figure 1) are maintained at the same potential, which is chosen by trial to give an appropriate separation between the sharp and broad peaks. Following the general procedure described by Hunt, Huffman, and McGee<sup>9</sup> we have derived an expression for the relation between the time separation of the precursor peak and the broad fragment ion peak,  $\Delta t$ , and the mass dif-

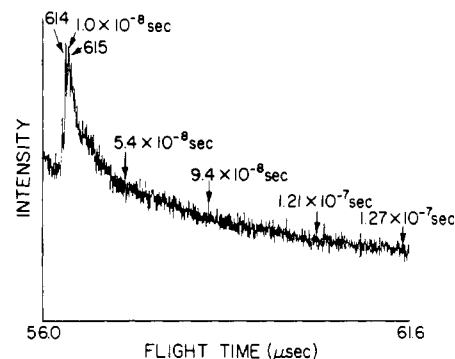


**Figure 3.** High-time tail on the  $m/z$  614/615 peak(s) resulting from the delayed-fragmentation reaction  $M^+/(M+1)^+ \rightarrow 614^+/615^+ + 278$ . The times given are the fragmentation delay times corresponding to the ions with flight times indicated by the arrows.

ference between the precursor ion and the fragment ion. This relation is

$$\Delta t = (M - \Delta M)^{1/2} \left[ \frac{K_1}{\left( \left( \frac{M - \Delta M}{M} \right) eV_s \right)^{1/2} + \left( \left( \frac{M - \Delta M}{M} \right) eV_s - eV_E \right)^{1/2}} + \frac{K_2}{\left( \left( \frac{M - \Delta M}{M} \right) eV_s - eV_E \right)^{1/2}} \right] - M^{1/2} \left[ \frac{K_1}{(eV_s)^{1/2} + (e(V_s - V_E))^{1/2}} + \frac{K_2}{(e(V_s - V_E))^{1/2}} \right] \quad (1)$$

where  $M$  = mass of precursor ion,  $\Delta M = M - M_f$ ,  $M_f$  = mass of fragment ion,  $V_s$  = potential of sample foil,  $V_E$  = potential of grids E and F,  $K_1 = 2^{1/2}(d_{DE} + d_{FG})$ ,  $K_2 = d_{EF}2^{-1/2}$ , and  $d_{IJ}$  = distance between grids I and J. The quantities  $K_1$  and  $K_2$  are evaluated as empirical constants. This was done by measuring the time of flight of an ion with given  $m/z$  using appropriate values of  $V_s$  and  $V_E$ . The flight time was then measured at two other values of  $V_E$  holding  $V_s$  constant. The three flight times for the three different retarding potentials provide two values of  $\Delta t$ . These and the appropriate values of  $V_s$  and  $V_E$  are substituted in eq 1 ( $\Delta M = 0$ ) to give a pair of simultaneous equations in  $K_1$  and  $K_2$ . This empirical procedure compensates for any errors in the distances  $d$  and higher order effects such as field penetration through the grids.

$\Delta t$  values were obtained by measuring the distance between the sharp and broad peaks on the mass spectrometer computer output as shown in Figure 2. Values of  $\Delta M$  are obtained from the experimental  $\Delta t$  values by iteration using eq 1.

Flight-tube fragmentations can be either spontaneous or collision induced. To determine which mechanism was involved in our retarding potential measurements, the pressure in the flight tube was varied. The retarding potential was set so that all ions were repelled. However, neutrals produced by flight tube fragmentations could still reach the detector and produce a neutral particle spectrum. The pressure in the flight tube was increased by a factor of 15 above its usual value of  $(3-5) \times 10^{-8}$  torr, but no change in the intensity of the neutral spectrum occurred in either the positive or negative mode of operation. Thus no collision-induced decomposition occurred in our retarding potential flight-tube fragmentation measurements.

Both the accelerating potential  $V_s$  and the retarding potential  $V_E$  were provided by highly regulated (0.01% stability) Spellman power supplies. The absolute values of these voltages were obtained using a precision voltage divider obtained from Julie Research Laboratories, Inc., New York, NY, (ratio tolerance = 0.015%) and a Fluke 8040A voltmeter (accuracy 0.05%). The largest uncertainty in the measurements was the determination of the center of the broad peak. Uncertainties in  $\Delta M$  values quoted in this paper reflect our estimates of the uncertainties in identifying these peak centers.

Ion fragmentations occurring in the acceleration region between the sample foil and the ground grid which serves as the entrance to the flight tube produce tails on the peaks in the time-of-flight mass spectrometer,<sup>8</sup> and these provide useful kinetic information. Ions produced by fragmentation of a precursor in the accelerating region receive from the accelerating field an amount of energy that varies with the point of fragmentation. The distribution of these points will result in a tail on

(9) Hunt, W. W.; Huffman, R. E.; McGee, K. E. *Rev. Sci. Instrum.* **1964**, *35*, 82.

(10) Graham, S. W.; Dowd, P.; Hercules, D. M. *Anal. Chem.* **1982**, *54*, 649.

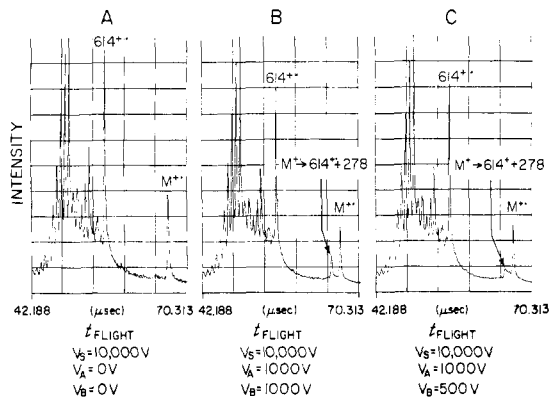


**Figure 4.** Illustration of peaks produced by delayed fragmentation occurring in a field-free or weak-field portion of the ion acceleration region: panel A, no field-free or weak-field portion; panel B, region between grids A and B (Figure 1) field free; panel C, weak field between grids A and B.

the sharp peak. This is illustrated in Figure 3. The sharp peak at  $m/z$  614 is a positive fragment ion that we suggest is produced by the loss with concomitant H-atom transfer of the phytol tail from the Chl *a* molecule. The  $m/z$  615 ion is probably a mixture of a  $^{13}\text{C}$  containing  $m/z$  614 ion and the protonated analogue of the  $m/z$  614 ion produced by decomposition of protonated Chl *a*. One observes that a perceptible tail extends for about  $5 \mu\text{s}$  beyond the sharp peaks. The times and arrows given in Figure 3 will be discussed later.

One can calculate the kinetic energy of an ion of mass  $M_f$  produced by fragmentation in the ion accelerating region of an ion of mass  $M$  at a time  $t_f$  after the initial formation of the ion of mass  $M$  on the sample foil. The time required for the fragment ion to traverse the flight tube,  $t_L$ , is related to its kinetic energy, and an expression relating  $t_f$  to the experimentally determined  $t_L$  can easily be derived. This expression is

$$t_f = \frac{Md_{SA}}{eV_s} \left[ \left( \frac{1}{M - M_f} \right) \left( 2eV_s - \frac{M_f L^2}{t_L^2} \right)^{1/2} \right] \quad (2)$$

where  $d_{SA}$  = distance between sample foil and grid A, which is maintained at ground potential, as are grids B and C,  $L$  = length of flight tube,  $V_s$  = voltage applied to sample foil, and the other terms are defined above. The times indicated on Figure 3 are  $t_f$  values calculated from  $t_L$  values with eq 2.

The sharp peaks in the spectrum have finite widths, and consequently the minimum delayed fragmentation time that produces ions distinguishable from prompt fragmentation ions is approximately  $1 \times 10^{-8}$  s.

Some experiments were made wherein voltages were applied to acceleration grids A and B (Figure 1), and this provided a segmented field between the sample foil and the ground grid entrance to the flight tube. If  $V_A = V_B$  the space between the two grids is field free, and all delayed fragmentations occurring between grids A and B will produce ions that will enter the flight tube with the same energy. These will comprise a peak in the mass spectrum, and the position of the peak between the parent ion peak and the prompt fragment ion peak will be determined by the value of  $V_s$  and  $V_A$ . Panel A of Figure 4 demonstrates a portion of the Chl *a* spectrum under source conditions where the ions are subjected to a uniform acceleration field. Note the absence of any significant peak between the  $M^+$  ion and the  $m/z$  614 $^+$  ion. Panel B shows the same portion of the Chl *a* spectrum when the ions are accelerated through a 9000-V potential drop between the sample foil and grid A, then drift without acceleration to grid B, and then are accelerated to ground. Immediately to the left of the  $M^+$  peak is a new peak that results from the fragmentation of  $M^+$  ions to  $m/z$  614 $^+$  ions in the region between acceleration grids A and B.

Of more interest is the case where a small potential is applied between grids A and B, and the results of this are illustrated in panel C (Figure 4). As in panel B the ions are initially accelerated by a 9000-V potential drop from the sample foil to grid A, but then they are accelerated by a 500-V potential difference between grids A and B before being finally accelerated to ground. Now fragmentations occurring between grids A and B will occur at slightly differing potentials depending on the positions/times of the fragmentations, and thus the energies with which they enter the flight tube will reflect these differences, which in turn will cause the flight times to reflect these different fragmentation positions/times. The sharp peak produced with no field between grids A and B (panel B, Figure 4) becomes a broader peak under the conditions of panel C, Figure 4. Since the fragmentations occurring between the two grids follow

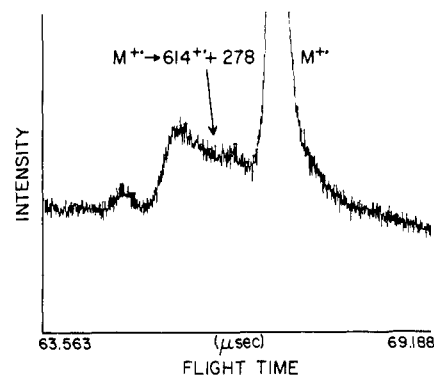


**Figure 5.** Expanded view of molecular-ion region of panel C, Figure 4.

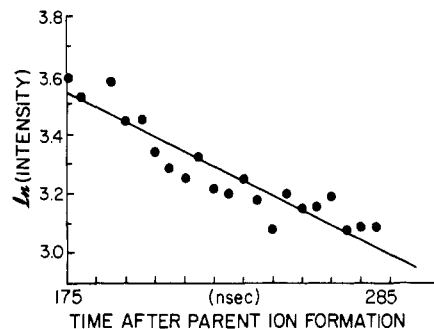


**Figure 6.** Semilog plot of intensity vs. time after parent ion formation for ions produced by the reaction  $M^+ \rightarrow 614^+ + 278$  comprising the broad peak in Figure 5.

first-order kinetics, a decrease in the amount of fragmentation as a function of distance/time between grids A and B is to be expected, and one observes that the broad decomposition peak in panel C exhibits such a diminution. This diminution is shown much more clearly in Figure 5, which is the molecular ion region of the spectrum given in Figure 4, panel C, on a larger scale.

We have derived a relationship between the flight times of ions appearing in the broad fragmentation peaks in Figure 4, panel C, and the time in the region between grids A and B at which the fragmentation occurred.

The considerations involved are analogous to those used in deriving eq 2. The relation obtained is

$$t_L = \left( \frac{M_f}{2 \left\{ \frac{M_f E_f}{M} + (eV_s - E_f) \right\}} \right)^{1/2} L \quad (3a)$$

where

$$E_f = e \left( \left( \frac{V_A - V_B}{d_{AB}} \right) \frac{t_f'}{(2M)^{1/2}} + (V_s - V_A)^{1/2} \right)^2 \quad (3b)$$

where  $d_{AB}$  = distance between grids A and B,  $t_f'$  = time of fragmentation after passing through grid A, and other symbols are as defined previously.

Equations 3a and 3b are solved for  $t_f'$  by iteration for various values of  $t_L$  along the broad decomposition peak. Intensities across this peak were corrected for any small peaks and irregularities in a background spectrum, which was taken from the spectrum produced with a uniform field in the ion acceleration region (panel A, Figure 4). A plot of the logarithm of the intensity as a function of the time after parent ion formation is given in Figure 6. These are the ions that undergo the fragmentation reaction  $M^+ \rightarrow 614^+ + 278$  in the region between grids A and B (Figure 1) under the conditions given in panel C, Figure 4.

## Results and Discussion

**A. Positive Spectra.** Positive and negative spectra of Chl *a* were taken under a variety of experimental conditions where the most important experimental variable was the retarding potentials applied at the end of the flight tube and in the acceleration region. Table I gives the positive ion spectrum obtained with a strong retarding potential applied after the flight tube. The sample foil

Table I. Positive Chl *a* Spectrum, Retarding Potential Applied<sup>a</sup>

<i>m/z</i>	RI, % base	<i>m/z</i>	RI, % base
23.985 <sup>b</sup>	100.0 <sup>c,d</sup>	425.21	3.7
24.989	22.8 <sup>d</sup>	426.24	3.1
25.986	17.3 <sup>d</sup>	427.18	2.5
27.017	20.4	435.17	2.2
29.040	14.7	436.21	2.7
38.005	5.7	437.25	4.0
39.019	31.8	438.20	4.3
41.032	33.2	439.24	6.3
43.048	25.8	440.19	4.8
51.012	20.6	441.24	3.4
52.017	6.5	449.16	2.1
53.005	16.9	450.22	2.8
55.057	25.6	451.17	5.3
57.080	10.7	452.23	6.0
62.006	9.1	453.19	8.9
63.012	16.3	454.25	6.7
65.018	6.5	455.21	4.9
69.074	6.4	456.18	2.9
73.070 <sup>e</sup>	51.7	465.20	4.4
74.009 <sup>e</sup>	15.0	466.27	4.8
75.011 <sup>e</sup>	14.1	467.24	10.0
77.013	8.6	468.22	8.0
87.010	7.3	469.19	5.8
111.01	2.6	470.17	3.4
115.05	2.6	480.30	2.5
133.03 <sup>e</sup>	2.2	481.29	14.2
147.11 <sup>e</sup>	16.8	482.28	12.0
148.14 <sup>e</sup>	4.2	483.27	9.6
149.11 <sup>e</sup>	2.6	484.15	6.1
207.12 <sup>e</sup>	2.4	485.14	3.8
221.25 <sup>e</sup>	2.0	614.37	2.9
410.19	2.2	615.36	3.2
411.20	2.4	616.36	2.8
412.21	2.2	892.66	0.17 (M <sup>+</sup> )
422.22	2.1	893.58	0.22 (M + 1) <sup>+</sup>
423.25	3.1	894.76	0.19 <sup>13</sup> C isotope
424.18	3.1	1786	0.08 } mixture of 2M <sup>+</sup>
		1787	0.08 } and (2M + H) <sup>+</sup>

<sup>a</sup> Notes: (1) Acceleration potential = 10.134 kV; retarding potential = 10.020 kV. (2) Minimum tabulated intensities: *m/z* 24–100, 5%; *m/z* 101–891, 2%; *m/z* ≥ 892, no limit. (3) Run time = 5.3 × 10<sup>4</sup> s. <sup>b</sup> Used as one point in a two-point mass calibration. H<sup>+</sup> used as other point. <sup>c</sup> Absolute intensity for this ion is 7.82 × 10<sup>5</sup> counts. This comprises 6.1% of total ionization. <sup>d</sup> Predominantly Mg isotopes. <sup>e</sup> Probably impurity ions.

was maintained at 10.134 kV; acceleration grids A and B and deceleration grids D and F (Figure 1) were at ground, and deceleration grid E was at 10.020 kV. Thus ions that lost more than 114 eV (1% of the initial energy) by decomposition in the flight tube were repelled. Fission fragment ionization spectra always exhibit a large, continuous background that may largely be attributed to ion decompositions during acceleration and to various random, uncorrelated ionization processes. This background has been subtracted from the results given in Table I and from other results to be given in this paper.

From Table I one sees that the most intense ion in the spectrum is the <sup>24</sup>Mg<sup>+</sup> ion. However, it comprises only 6% of the total ionization in the spectrum, and one concludes that extensive fragmentation occurs in the positive ionization of Chl *a* by fission fragment bombardment.

The spectrum in Table I comprises a number of regions of interest. The molecular ion region consists of a trio of peaks of about equal intensity. The (M + 1)<sup>+</sup> ion at *m/z* 893.58 is the most intense ion in this region of the spectrum. The relative intensity of the M<sup>+</sup> ion at *m/z* 892.66 is 0.17, and using the natural isotopic abundances for the elements in chlorophyll one calculates that the intensity of the (M + H)<sup>+</sup> ion at *m/z* 893.58 is 0.089; i.e., the intensity of protonated Chl *a* is 52% that of the Chl *a* molecule ion, M<sup>+</sup>. The presence of (M + H)<sup>+</sup> ions in the Chl *a* spectrum has not been reported previously by other workers.

A second region consists of three ions of approximately equal intensity at *m/z* 614, 615, and 616, and these are probably as-

Table II. Positive Chl *a* Spectra, Percent Total Ionization

mass range	% total counts	
	ret pot. applied <sup>a</sup>	ret pot. not applied <sup>b</sup>
24–100	48.1	20.2
101–410	21.7	15.5
411–485	24.8	31.7
486–610	3.4	18.9
611–618	1.6	8.5
891–896	0.12	5.1

<sup>a</sup> Total counts = 1.29 × 10<sup>7</sup>. Irradiation time = 5.26 × 10<sup>4</sup> s.

<sup>b</sup> Total counts = 2.23 × 10<sup>7</sup>. Irradiation time = 4.22 × 10<sup>4</sup> s.

sociated with the loss of the phytol tail from the chlorophyll ion. A more interesting region extends from *m/z* 410 to 485. An ion occurs at every mass number, but a periodic variation in intensity occurs to produce clusters of peaks separated by about 14 mass units. Virtually no ions of interest occur in the range *m/z* 100–400. A number of ions of high intensity are observed in the range *m/z* 24–100, and as we pointed out above, the Mg<sup>+</sup> ion at *m/z* 24 is the most intense in the spectrum. The exact masses indicate that many of the ions in this mass range contain appreciable amounts of hydrogen, and thus they are organic ions mostly formed from Chl *a*. However, we believe that several of the ions in Table I are produced from impurities. Ions at the masses indicated in Table I as impurity masses are frequently observed in chlorophyll samples and in samples of other materials that we have examined mass spectrometrically. We suspect the ions at *m/z* 73, 133, 147, 207, and 221 to be silicon-containing ions, probably derived from siliconizing compounds used in the course of the manufacture and/or subsequent handling of the chlorophyll. We are confirmed in this view by the fact that the spectrum of an authentic siliconizing reagent (Pierce DRI-FILM SC-87) produced these ions and in about the same intensities we found in the Chl *a* sample.

In the positive spectrum obtained without retarding potential many broad peaks are observed. The molecular ion region consists of a broad peak with a width of approximately 18 mass units and little or no unit-mass fine structure. In the region between *m/z* 500 and 620 peaks appear that are 10–14 mass units wide at the base, and they also show no fine structure corresponding to unit mass resolution. The application of retarding potential suppresses these peaks so strongly that the intensities of the peaks other than that at *m/z* 615 are too small to be included in Table I. The breadths of these peaks mean that the ions producing them have undergone decompositions in the flight tube. On the other hand, no particular difference in the appearance of the peaks in the low-mass end of the spectrum (*m/z* < 100) is to be observed with and without the retarding voltage, which indicates that these ions do not undergo much in-flight fragmentation.

Because of the extensive overlap of adjacent peaks and the much degraded resolution in the high-mass portion of the spectrum obtained without the retarding potential, a tabulation of the unretarded spectrum on a unit mass basis is not appropriate. Thus we give in Table II, column 3, the unretarded relative intensities summed over several mass ranges. For comparison we give in column 2 of Table II the relative intensities summed over the same mass ranges for the retarded spectrum. The retarded and unretarded summed spectra are quite different, with low-mass ions in greater preponderance in the retarded spectrum. This is evidence that high-mass ions undergo more fragmentation in the flight tube than low-mass ions, which conclusion was also reached from peak-breadth evidence discussed above.

It is of interest to get quantitative information about the fraction of the ions in the several mass regions which fragment in the flight tube, and this can be done by comparing absolute intensities with and without retardation. Such data are given in Table III. Only 1.1% of the ions in the molecule-ion region (*m/z* 891–896) that enter the flight tube live long enough to reach the detector, and 8.3–8.5% of the ions with masses between *m/z* 486 and 618 entering the flight tube reach the detector. The lifetimes of smaller ions are greater, and Table III shows that ions in the range *m/z*

Table III. Positive Chl *a* Spectra, Absolute Intensities

mass range	10 <sup>-6</sup> counts <sup>a</sup>		<i>R</i> <sup>b</sup>
	with 10-kV ret pot.	without ret pot.	
24-100	4.97	4.50	110.0
101-410	2.25	3.46	65.0
411-485	2.57	7.07	36.4
486-610	0.35	4.22	8.3
611-618	0.16	1.89	8.5
891-896	0.012	1.14	1.1

<sup>a</sup> Normalized to be the counts obtained in  $4.22 \times 10^4$  s of bombardment. <sup>b</sup>  $R = 100[\text{counts (with retarding potential)}/\text{counts (without retarding potential)}]$ .

24-100 do not undergo appreciable fragmentation in the flight tube. The fact that the intensity of ions in this range with retarding potential is slightly higher than the intensity of those without retarding potential is probably the result of experimental error. The extensive fragmentation observed here in Chl *a* has been found previously in this laboratory with other compounds.<sup>7</sup>

We wish to discuss several physical considerations that affect the spectra obtained in time-of-flight mass spectrometers with and without retarding potential. With a retarding potential such as that used for the spectrum in Table I, virtually all of the fragmentations occurring in the flight tube will be rejected and will not contribute to any portion of the spectrum. The flight tube is approximately 3 m long, and at the 10-kV accelerating voltage used in our experiments, 67.5  $\mu$ s is required for the molecule ions of Chl *a* to reach the detector. However, the flight times and thus the lifetimes required for the collection of an intact fragment ion will be less by an amount depending upon the mass of the ion. The consequences of this set of circumstances is that the spectrum obtained for any compound will be very instrument specific, depending quite strongly on the length of the flight tube and the acceleration voltage used. Furthermore, the spectrum obtained experimentally reflects a very complicated set of properties of the sample; namely, it depends upon the numbers of different ions that are produced in a relatively short time after the ionizing event (prompt fragmentations) and upon the minimum lifetimes required of these ions for collection, which are mass related.

In the absence of retarding potential, ions that undergo decomposition in the flight tube are collected at the same time as unfragmented ions, although the release of small amounts of kinetic energy in the fragmentation process broadens the peaks. Thus a spectrum obtained without retardation, such as the summed spectrum given in Table II, column 3, represents the distribution of the intensities of ions entering the flight tube of the mass spectrometer. The transit time of the ion acceleration region for our mass spectrometer at 10-kV ion acceleration voltage ranges from 5 ns for an ion of  $m/z$  1 to 151 ns for an ion with  $m/z$  892. Thus the unretarded spectrum gives the ion distribution at times on the order of 10-100 ns after the initial ionizing event. Such spectra will primarily reflect the initial distribution of molecule ions and fragment ions, and this is information not normally obtained in mass spectrometry. In a 12-in. radius of curvature double-focussing magnetic deflection instrument the ion path length is on the order of 5-7 ft, and at 8-kV ion accelerating voltage the time required for an  $m/z$  892 ion to transit the mass analyzer is 37-51  $\mu$ s. Ions undergoing decomposition in approximately 80% of this flight path will not contribute to the sharp peaks that comprise the major part of the spectra of such instruments, and thus these spectra result from ions which must live for times up to 30-40  $\mu$ s. Furthermore, several microseconds are required to accelerate ions from their point of formation to the mass analyzer. Thus the situation which obtains with such a mass spectrometer is very similar to that obtaining with our time-of-flight instrument with retarding potential applied; that is, a spectrum reflects some combination of initial ion formation plus long-time stability. For quadrupole mass spectrometers a typical ion transit time is even longer (100-200  $\mu$ s). The relatively small dependence of an unretarded time-of-flight spectrum on long-time

Table IV. Negative Chl *a* Spectrum, Retarding Potential Applied<sup>a</sup>

$m/z$	RI, % base	$m/z$	RI, % base
25.008 <sup>b</sup>	26.6	466.39	0.30
26.009	100.0 <sup>c</sup>	467.34	0.73
49.007	22.9	468.31	0.57
50.007	21.2	469.28	0.53
65.026	12.2	470.35	0.40
66.008	5.4	481.36	0.54
73.011	14.1	482.35	0.44
74.004	9.7	483.33	0.39
97.012	6.7	525.36	0.21
101.02	8.1	526.38	0.25
102.01	17.8	527.40	0.28
103.02	4.2	540.45	0.25
104.01	2.6	541.38	0.29
121.02	3.0	542.41	0.20
125.03	3.9	613.46	0.43
126.03	3.2	614.44	0.37
451.53	0.23	615.42	0.25
452.48	0.30	891.54	0.03 (M - 1) <sup>-</sup>
453.53	0.35	892.58	0.09 M <sup>-</sup>
454.48	0.27	893.52	0.12 (M + 1) <sup>-</sup>
455.54	0.30	894.56	0.09
456.49	0.20	895.49	0.07
465.32	0.24		

<sup>a</sup> Notes: (1) Acceleration potential = 10.113 kV; retarding potential = 9.455 kV. (2) Minimum tabulated intensities:  $m/z$  24-100, 5%;  $m/z$  101-200, 2%;  $m/z$  201-891, 0.2%;  $m/z \geq 892$ , no limit. (3) Run time =  $4.23 \times 10^3$  s. <sup>b</sup> Used as one point in a two-point calibration. H<sup>-</sup> used as other point. <sup>c</sup> Absolute intensity for this ion is  $6.82 \times 10^5$  counts. This comprises 16.3% of total ionization.

Table V. Negative Chl *a* Spectra, Percent Total Ionization

mass range	% total counts	
	ret pot. applied <sup>a</sup>	ret pot. not applied <sup>b</sup>
25-100	68.2	54.6
101-410	26.1	25.9
411-500	3.5	6.5
501-610	1.5	6.3
611-622	0.5	3.3
890-896	0.15	3.4

<sup>a</sup> Total counts =  $4.02 \times 10^6$ . Irradiation time =  $4.23 \times 10^3$  s.

<sup>b</sup> Total counts =  $9.97 \times 10^6$ . Irradiation time =  $8.55 \times 10^3$  s.

ion stability may be of analytical utility.

**B. Negative Spectra.** The negative Chl *a* spectrum obtained with retarding potential applied is given in Table IV, and the retarded spectrum obtained by summing the intensities in several mass regions is given in Table V, column 2. The unretarded spectrum obtained by summing the intensities in several mass regions is given in Table V, column 3. For retarded spectra the sample foil was maintained at -10.113 kV, acceleration grids A and B and deceleration grids D and F (Figure 1) were at ground, and deceleration grid E was at -9.455 kV. The retardation for the negative ion spectrum was less than that for the positive spectrum because voltage breakdown in the retarding grid assembly seemed to set in at lower voltages in the negative case than in the positive case. The suppression of peaks corresponding to flight-tube fragmentation ions was in some cases not complete in the negative ion spectrum, but this causes no serious problems of understanding the spectrum.

In the negative spectrum, as in the positive spectrum, the most intense ion is a low-mass ion, namely,  $m/z$  26 in the negative spectrum, and this ion comprises 16% of the total ionization. The intense formation of this ion in the negative fission fragment ionization spectra of nitrogen-containing compounds has already been reported,<sup>7</sup> and it is also found in laser desorption mass spectra of nitrogen-containing organic compounds.<sup>10</sup> From the exact mass of the  $m/z$  26 peak and from previous experiments, this ion is CN<sup>-</sup>.

The molecule-ion region in the retarded spectrum consists of a set of five peaks with  $m/z$  891, 892, 893, 894, and 895.  $m/z$

Table VI. Negative Chl *a* Spectrum, Absolute Intensities

mass range	10 <sup>-6</sup> counts <sup>a</sup>		<i>R</i>
	with 9.455-keV ret pot.	without ret pot.	
25-100	2.74	2.69	102
101-410	1.05	1.28	82
411-500	0.14	0.32	44
501-610	0.06	0.31	19
611-622	0.02	0.16	12
890-896	0.006	0.17	3.6

<sup>a</sup> Normalized to the counts obtained in  $4.23 \times 10^3$ s of bombardment. <sup>b</sup>  $R = 100[\text{counts (with retarding potential)}/\text{counts (without retarding potential)}]$ .

892.58 is primarily the negative molecule ion,  $M^-$ , and if one corrects the intensities of the  $(M-1)^-$ ,  $M^-$ , and  $(M+1)^-$  ions for naturally occurring higher mass isotopes, one calculates that the  $M^-$  ion is the most intense ion in the molecule-ion region, followed by the  $(M+H)^-$  ion with an intensity 87% that of  $M^-$ , followed by the  $(M-H)^-$  ion with 44% the  $M^-$  intensity. The presence of  $(M+H)^-$  ion has not previously been reported by other workers.

From Table V, column 2, and Table II, column 2, one sees that the molecule-ion region contains about the same small percent of the total ionization in both the negative and positive spectra of Chl *a*.

Table VI gives the summed spectra utilizing absolute intensities for negative ions with and without retarding potential. Fractions of ions in the several mass regions that fragment in the flight tube are also given. As was the case with positive ions, the larger the ion entering the flight tube, the greater is the amount of decomposition occurring in the flight tube.

As we have pointed out, extensive fragmentation occurs in both the positive and negative spectra of Chl *a*. However, the amount is greater in the negative case, and the ion distribution as a function of mass is different in the two cases. From Tables II and V one can calculate that the fraction of the total ionization with  $m/z > 411$  without retardation is 64.2% for positive ions and 19.5% for negative ions. Thus much more prompt fragmentation occurs with negative ions. The mass range that shows the greatest difference is  $m/z$  411-485 (positive), corresponding to  $m/z$  411-500 (negative). The former contains 31.7% of the total positive ionization, but the latter contains only 6.5% of the negative ionization. These mass ranges correspond to ions in which the macrocyclic ring in Chl *a* is largely or completely intact, and we interpret the difference in intensities in these ranges as meaning that in the negative case the macrocyclic ring undergoes more prompt fragmentation than in the positive case. Conversely, the negative intensity in the range  $m/z$  25-100 is 54.6%, whereas the positive intensity in the range  $m/z$  24-100 is 20.2%. The difference may be attributed to the large intensity of the  $m/z$  26 ( $CN^-$ ) ion in the negative spectrum. We suggest that the negative spectrum of Chl *a* is determined very extensively by a strong and not understood tendency of the macrocyclic ring to undergo a rapid and complicated decomposition to give  $CN^-$ .

In some of our Chl *a* samples appreciable amounts of pheophytin *a* were present. The molecular weight of pheophytin is 868.55, and the mass spectrum of Chl *a* in this region is devoid of peaks; consequently, a good spectrum of the molecule-ion region of pheophytin *a* can be obtained. The molecule-ion regions of the positive and negative spectra of pheophytin *a* are given in Figure 7. Two points of interest occur in the comparison of the pheophytin *a* spectra and the Chl *a* spectra. First, comparing Figure 7 with the negative spectrum of Chl *a*, one sees quite a marked difference in the relative intensities of the several peaks. Making the appropriate corrections for naturally occurring higher mass isotopes, one obtains the result that in pheophytin *a* the  $M^-$  ion ( $m/z$  896) has a relative intensity of 100, the  $(M-1)^-$  ion ( $m/z$  868) has relative intensity 34, and the  $(M+1)^-$  ( $m/z$  870) has a relative intensity of 22. Thus the relative intensity of the  $(M+1)^-$  ion in pheophytin *a* is much smaller than that in Chl

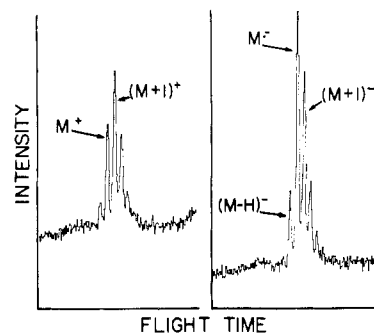


Figure 7. Molecule-ion regions of positive and negative spectra of pheophytin *a*. Retarding potential applied.

*a*. Second, determination of the summed intensities in the molecule-ion regions of pheophytin *a* with and without retarding potential give the result that 13% of the positive ions and 26% of the negative ions that enter the flight tube of the mass spectrometer survive to reach the collector. These figures are significantly larger than the corresponding figures for Chl *a*, which from Tables III and VI are 1.1 and 3.6%, respectively.

The transfer of a hydride ion to form an  $(M+H)^-$  ion has been reported in gas-phase anionic chemistry.<sup>11</sup> The presence of the magnesium in Chl *a* provides additional orbitals for bonding an  $H^-$  ion that are not present in pheophytin *a*, and this rationalizes the higher  $(M+H)^-$  intensity of Chl *a*.

Chl *a* is known to form association entities both in condensed and gas phase, and the binding involved in these adducts is considered to involve interaction between vacant orbitals on the magnesium atom of one chlorophyll molecule and lone-pair electrons on the carbonyl group of a second chlorophyll molecule.<sup>1,12,13</sup> It has been found<sup>1</sup> that while Chl *a* ions produced by fission fragment ionization associate with Chl *a* molecules to form dimers and higher association ions, pheophytin *a* ions do not associate with pheophytin *a* molecules. The nonassociation in pheophytin *a* is attributed to the absence of the magnesium atom as the site for the associative binding. Our finding concerning the relative intensities of  $(M+H)^-$  ions in Chl *a* and pheophytin *a* is in accord with these prior findings and ideas.

Pheophytin *a* molecule ions exhibit less fragmentation in the flight tube of the mass spectrometer than does Chl *a*, and other observations on pheophytin *a* indicate that fragmentation in this molecule is in general less than that in Chl *a*. A possible explanation for this behavior is that the strong interaction involving the magnesium makes Chl *a* less volatile than pheophytin *a*, and thus more energy has to be introduced into Chl *a* to produce gaseous ions. Some of this extra energy will make its way into vibrational modes, producing greater fragmentation.

**C. Retarding Potential Measurements.** Retarding potential studies designed to elucidate fragmentations in the flight tube were made for 13 ionic fragmentations in the positive spectrum of Chl *a* and for 9 fragmentations in the negative spectrum. These were all of the fragmentations that occurred with sufficient intensity to permit quantitative investigation. For some precursor ions it was possible to deduce the occurrence of several fragmentation processes occurring from the same precursor ion. In these cases it was found that the application of a continually increasing retarding potential would effect the sequential separation of several broad peaks corresponding to the different fragmentation processes. These sequential broad peaks move in order away from the sharp peak as the retarding potential is increased, and at appropriate potentials they disappear as the retarding potential completely stops the travel of the ions to the detector. It proves to be quite feasible to make quantitative measurements on each

(11) DePuy, C. H.; Bierbaum, V. M.; Schmitt, R. J.; Shapiro, R. H. *J. Am. Chem. Soc.* **1978**, *100*, 2920.

(12) Katz, J. J.; Closs, G. L.; Pennington, F. C.; Thomas, M. R.; Strain, H. H. *J. Am. Chem. Soc.* **1963**, *85*, 3801.

(13) Anderson, A. F. H.; Calvin, M. *Arch. Biochem. Biophys.* **1964**, *107*, 251.

Table VII. Flight-Tube Decomposition Data for Positive Ions

precursor ion	acceleration voltage <sup>a</sup>	deceleration voltage	$\Delta t$ , ns	$\Delta M$ , amu	% of fragmentation detected
1787	10135	4711	973 ± 56	894 ± 6	57
892 or 893	10137	6511	624 ± 20	279 ± 2	56
614 or 615	10134	7414	444 ± 5	133 ± 1	49
614 or 615	10137	8715	427 ± 30	61 ± 2	33
614 or 615	10135	9331	422 ± 30	30 ± 1	3
555	10134	8119	468 ± 60	88 ± 3	37
555	10134	8119	878 ± 80	100 ± 2	38
555	10135	8422	502 ± 25	74 ± 1	41
540	10137	8715	546 ± 42	60 ± 2	41
481	5511	5062	807 ± 80	30 ± 1	12
481	5511	5210	503 ± 70	15 ± 1	21
467	5511	5210	472 ± 70	14 ± 1	27
453	5511	5210	578 ± 80	15 ± 1	25

<sup>a</sup> For measurements with acceleration voltage = 10 kV,  $K_1$  and  $K_2$  (eq 1) are:  $K_1 = 2.478$  and  $K_2 = 0.725$ . For measurements with acceleration voltage = 5.5 kV,  $K_1 = 2.443$  and  $K_2 = 0.712$ .

Table VIII. Flight-Tube Decomposition Data for Negative Ions

precursor ion	acceleration voltage <sup>a</sup>	deceleration voltage	$\Delta t$ , ns	$\Delta M$ , amu	% of fragmentation detected
1787	10110	4909	1694 ± 75	895 ± 2	90
892, 893	10110	6528	675 ± 28	281 ± 2	61
613, 614	10110	8541	552 ± 45	75 ± 2	56
613, 614	10110	8541	1025 ± 80	86 ± 1	25
540, 541	10113	8541	358 ± 30	58 ± 2	53
540, 541	10113	9455	248 ± 50	16 ± 2	14
526, 527	10111	8541	394 ± 40	59 ± 2	63
481	10113	9455	233 ± 25	14 ± 1	65
467	10113	9455	231 ± 25	14 ± 1	55

<sup>a</sup> For all measurements  $K_1$  and  $K_2$  (eq 1) are  $K_1 = 2.478$  and  $K_2 = 0.725$ .

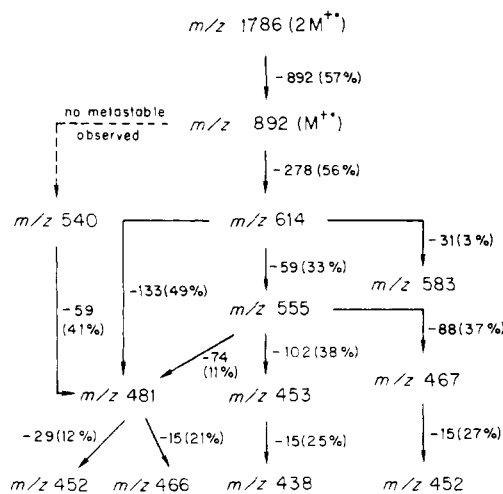
of these peaks and thus to determine the identities of the several processes proceeding from a given precursor ion.

Table I shows that both  $M^+$  and  $(M + H)^+$  ions are present in the positive spectrum of Chl *a*. Our retarding potential measurements do not have sufficient resolution to distinguish between these ions, so the two are considered together. Similar uncertainties exist for several other ions.

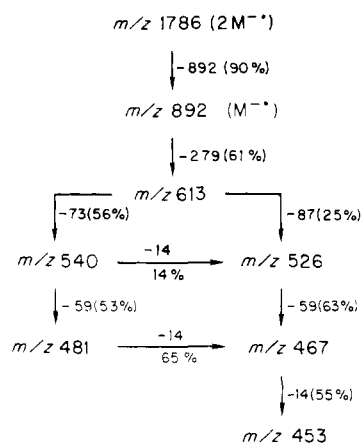
Table VII gives the retarding potential results obtained for the positive Chl *a* spectrum. Completely analogous considerations apply for the negative spectrum, and retarding potential results for the negative Chl *a* spectrum are given in Table VIII.

Measurements of the intensities of the peaks involved in these fragmentations give useful information. For a given fragmentation, the number of counts in the broad peak before the application of a retarding potential is measured, as is the number of counts in the broad and sharp peak produced by the application of the retarding potential. When the retarding potential produces a sharp peak and more than one broad peak, the number of counts in each broad peak is measured. We let  $B_0$  be the counts in the broad peak without retarding potential,  $B_r$  be the counts in the broad peak with retarding potential, and  $S$  be the number of counts in the sharp peak with retarding potential. Then we define the percent of decomposition detected as  $100B_r/(B_0 - S)$ . This quantity is given in the rightmost columns of Tables VII and VIII. Values of less than 100 indicate that fragmentations are occurring that we do not detect for reasons of intensity or interferences. When several fragmentations from a given precursor ion occur, the percent fragmentation detected for each fragmentation can be used to calculate an approximate branching ratio for the fragmentation of the precursor. The branching ratios become

Scheme I



Scheme II



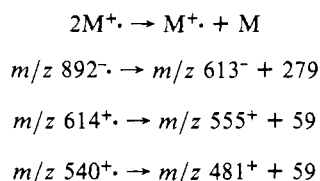
exact if the sum of the percent fragmentation detected is 100%.

**D. Fragmentation Paths (Positive Ions).** The retarding potential results given in Table VII permit one to deduce the network of fragmentations occurring for Chl *a* positive ions in the flight tube of the mass spectrometer, and this is given in Scheme I. We pointed out earlier that fragmentations could start from either the  $M^+$  ion or the  $(M + H)^+$  ion, and our retarding potential measurements do not enable us to distinguish between these two possibilities. Fragmentations from these two ions can produce ions at  $m/z$  614 and 615, respectively, for example, and this cannot be distinguished either. Such uncertainties exist for several ions in the overall fragmentation scheme. To simplify our presentation, we give in Scheme I only the  $m/z$  values that correspond to the lower of the pairs of  $m/z$  possibilities, and this corresponds formally to considering only the decompositions starting with  $M^+$ . However, it should be kept in mind that a network involving  $(M + H)^+$  ions as a precursor probably exists.

**E. Fragmentation Paths (Negative Ions).** Scheme II gives the network of flight tube of decompositions deduced for negative ions from the retarding potential data given in Table VIII. As was the case with the positive ion decomposition network, we include in Scheme II only decompositions starting from and involving the  $M^-$  ion, and it should be kept in mind that sequences involving the  $(M + H)^-$  and the  $(M - H)^-$  ions may occur.

**F. Kinetic Results.** Figure 3 shows the tail directed toward longer flight times on the  $m/z$  614/615<sup>+</sup> peak. As we explained earlier in the Experimental Section, this tail results from  $m/z$  892/893 ( $M^+$  or  $(M + H)^+$ ) ions fragmenting to  $m/z$  614/615<sup>+</sup> ions in the ion accelerating region. The time after the ionizing event at which fragmentation occurs can be calculated from the flight time by means of eq 2. The times written above the arrows in Figure 3 are the fragmentation times at five different flight times. One sees from this figure that there is a continuous range

of fragmentation times between  $1 \times 10^{-8}$  s, which is the shortest fragmentation time that can be detected by this method, and  $1.27 \times 10^{-7}$  s. A continuous decrease in the intensity occurs over the length of the tail, which indicates in a qualitative way that a diminishing number of fragmentations occurs with increasing time after initial ionization, which is the behavior to be expected for a first-order reaction. However, a falling background intensity resulting from instrumental causes is often also to be observed, and consequently utilizing the time-dependent intensity diminution in Figure 3 to obtain quantitative fragmentation rate constants would be subject to error. The diminution of the intensity of the tail becomes indistinguishable from background approximately at the right-hand margin of Figure 3, and thus this constitutes a limit to the detectable times of fragmentation in the acceleration region. However, we pointed out earlier that the ion transit time of an  $M^+$  ion ( $m/z$  892) through this region in our instrument with an ion accelerating voltage of 10 kV (the voltage used in obtaining Figure 3) is  $1.51 \times 10^{-7}$  s, and thus we can detect fragmentations occurring across most of the ion accelerating region. Tails such as that in Figure 3 can be detected only on peaks in the spectrum which are sufficiently separated from adjacent higher mass peaks that interferences do not occur. This limits the number of tails in a spectrum that can be studied. In Chl *a* we have found tails like that in Figure 3 for the reactions



While we cannot quantitatively determine rate constants from plots such as Figure 3, it is clear that significant amounts of reaction occur in times between  $10^{-8}$  and  $10^{-7}$  s, and this is compatible with rate constants of  $\sim 10^7$  s $^{-1}$ .

To obtain more quantitative fragmentation rate information we make use of the experiment described previously where appropriate potentials are applied to grids A and B (Figure 1). The potential applied to grid B is slightly lower than that applied to grid A, and consequently the ions are accelerated slowly between the two grids. Fragmentations occur during this transit time, and the fragmentation times can be determined. It now is possible to make reliable background corrections, and thus we can plot intensity against time after the initial ionizing event. A semilog plot of intensity vs. time for the reaction  $m/z\ 892(M^+) \rightarrow m/z\ 614^+ + 278$  is given in Figure 6. The slope of this plot yields the value  $(4.4 \pm 0.4) \times 10^6$  s $^{-1}$  for the rate constant of the reaction in the time window between 175 and 285 ns. In a conventionally obtained time-of-flight spectrum, i.e., one with zero potential applied to grids A and B, this would be the rate constant for the

fragmentation of the molecule ion in the first part of the flight tube.

Our experimental results provide evidence for the occurrence of reactions with a range of reaction rates. We find molecule ions that fragment rapidly enough to produce sharp fragment ions, and such fragmentations must be completed before the molecule ion has moved very far from the sample foil, i.e., within a time of a few nanoseconds or less. The rate constants for these must be  $10^9$  s $^{-1}$  or greater. The tails on fragment peaks represent reactions with rate constants of  $10^8$ – $10^7$  s $^{-1}$ . Ions decomposing with a rate constant of  $4.4 \times 10^6$  s $^{-1}$  in the first part of the flight tube will have completely decomposed after a few microseconds (after  $5 \mu\text{s } I/I_0 = 2 \times 10^{-10}$ ), but experimentally we find that a finite number of chlorophyll molecule ions live for at least 67.5  $\mu\text{s}$  and reach the ion detector. Thus chlorophyll molecule ions decomposing with rate constants much smaller than  $4.4 \times 10^6$  s $^{-1}$  must also be produced by the initial ionization. We think that fragmentations occur along the length of the flight tube, but with the rate of fragmentation decreasing as the tube is traversed. Consequently, we postulate that some Chl *a* molecule ions have fragmentation rate constants an order of magnitude or more smaller than  $4.4 \times 10^6$  s $^{-1}$ . Our results are therefore compatible with Chl *a* molecule-ion fragmentation rate constants ranging from  $10^9$  s $^{-1}$  to perhaps  $10^4$  s $^{-1}$ . The experiments we have done to get information about fragmentation rate constants have mostly been done on positive ions, although we have experimentally observed extensive flight-tube fragmentation for negative ions. Thus our conclusion about the range of decomposition rates strictly speaking applies only to positive ions, but in fact the overall behavior of the positive and negative ions from Chl *a* is similar enough to cause us to suggest that the same general kinetic considerations apply to both kinds of ions.

The behavior we observe is compatible with chlorophyll ions being formed in the initial volatilization–ionization process with a distribution of excitation energies, and these differing excitation energies will produce fragmentations proceeding at differing rates. Our findings lead us to suggest that the fission fragment-induced fragmentation processes observed in Chl *a* involve many of the concepts embodied in the quasi-equilibrium theory of mass spectra, e.g., the formation of reactant ions with a wide range of energies, which results in a network of sequential and competing unimolecular reactions with variable and wide-ranging rate constants. This view is contrary to the hypothesis advanced by Hunt and co-workers<sup>2</sup> that fragmentation in the fission fragment ionization of mass spectrometry of Chl *a* occurs exclusively in a very short time ( $10^{-12}$ – $10^{-14}$  s).

**Acknowledgment.** This work was supported in part by the Division of Research Resources, National Institutes of Health. We thank Gladys Roberts for help in preparing the manuscript.

**Registry No.** Chlorophyll *a*, 479-61-8.